JOURNAL OF MATERIALS SCIENCE **35** (2000) 1925–1930

Microstructure and mechanical properties of TiC-Ni functionally graded materials by simultaneous combustion synthesis and compaction

XING-HONG ZHANG
Center for Composite Materials, Harbin Institute of Technology, Harbin 150001, People's Republic of China

JIE-CAI HAN
Center for Composite Materials, Harbin Institute of Technology, Harbin 150001, People's Republic of China; Department of Materials Engineering and Materials Design, University of Nottingham, UK

SHAN-YI DU
Center for Composite Materials, Harbin Institute of Technology, Harbin 150001, People's Republic of China

J. V. WOOD*
Department of Materials Engineering and Materials Design, University of Nottingham, UK

The simultaneous combustion synthesis and hot compaction of Ti, C and Ni powders under a hydrostatic pressure was undertaken to fabricate fully dense TiC-Ni functionally graded materials (FGM) in a single processing operation. The composition gradient was optimized by finite element analysis and obtained by stacking different powder mixtures of desired compositions. X-ray diffraction, scanning electron microscopy and microprobe analysis were employed to investigate the crystalline phase, microstructure and Ni distribution. Experimental results demonstrate that the combustion reaction was complete and the final products contained the phases TiC and Ni only, the microstructure varies coherently throughout the specimen with no distinct interface. The physical and mechanical properties were measured as a function of composition. It was found that the properties of the FGMs were dependent on the Ni content and approached the maximum values for the relative density, hardness and flexural strength at room temperature when the Ni content was increased to 20 wt%. The maximum in fracture toughness value was found in the TiC-30 wt% Ni material.

1. Introduction

The synthesis of functionally graded materials (FGMs) has been successfully demonstrated through a variety of methods, including thermal spray, powder metallurgy, physical and chemical vapor deposition, and self-propagating high-temperature synthesis (SHS) or combustion synthesis [1–3]. Among these, SHS methods are advantageous owing to the lower cost and better availability of starting materials, simple processing equipment, lower energy consumption and shorter processing times. Recently, the rapid development of SHS has provided a good option for the fabrication of thicker, net shape or near net shape FGM components. In this respect, various researchers [4–7] have studied synthesis of FGMs using the Ti-B-Cu, Ti-C-Ni and Ti-C-Cu systems. By combining combustion synthesis and a hot forming process, Sata *et al*. [4] and Ma *et al*. [5] have obtained near-fully dense TiB_2-Cu and TiC-Ni FGMs. Kudesia *et al*. [6] studied a TiC-NiAl FGM system as a method of joining a ceramic (TiC) and an intermetallic compound (NiAl). Shon and Munir [7] have investigated the synthesis of TiC-Cu FGMs by electrothermal combustion. Another variation of the SHS; namely the reaction hot compaction technique, has been successfully used by Padmavardhani *et al*. [8] to produce dense NiAl-Al_2O_3 FGMs. In this paper, the combustion synthesis and densification, microstructure and properties of a TiC-Ni FGM have been explored.

* Author to whom all correspondence should be addressed.

2. Experimental procedure

High-purity (>99.5%) powders of elemental titanium, carbon and nickel were used in this investigation. The particle sizes for Ti, C and Ni powders were 44 μm (−325 mesh), 44 μm and 52 μm, respectively. Reactant mixtures were mixed in a dry mixer for 24 h and subsquently dried in a vacuum oven for 24 h at 363 K, these powders were compacted in a stainless steel die with double-acting rams to form the samples. The green density of the compacts was maintained at about 52% of theoretical. Simultaneous combustion synthesis and compaction was accomplished utilizing a 200t hydrostatic press. Fig. 1a is a schematic illustration of the simultaneous combustion synthesis and compaction technique showing some of its pertinent features. The flow chart for manufacturing a FGM via simultaneous combustion synthesis and compaction is shown in Fig. 1b. The powder compacts were 70×70 mm in section and approximately 30 mm in height (Fig. 1c) were contained in a special die. The die was designed such that it can confine the material during reaction and densification while allowing the expulsion of volatile impurity gases evolved during the reaction. The compact behaves as a porous viscous body during densification and is contained by surrounding it with sand. The sand also acts as a pressure-transmitting medium creating a macroscopic quasi-isostatic state of stress on the compacts. The dense TiC-Ni FGM and non-FGMs with various compositions were then sectioned for microstructure and mechanical property analysis. Analysis of the product was made by X-ray diffraction (XRD), scanning electron microscopy (SEM) and microprobe analysis (EPMA). The mechanical properties were measured for the composites as a function of composition.

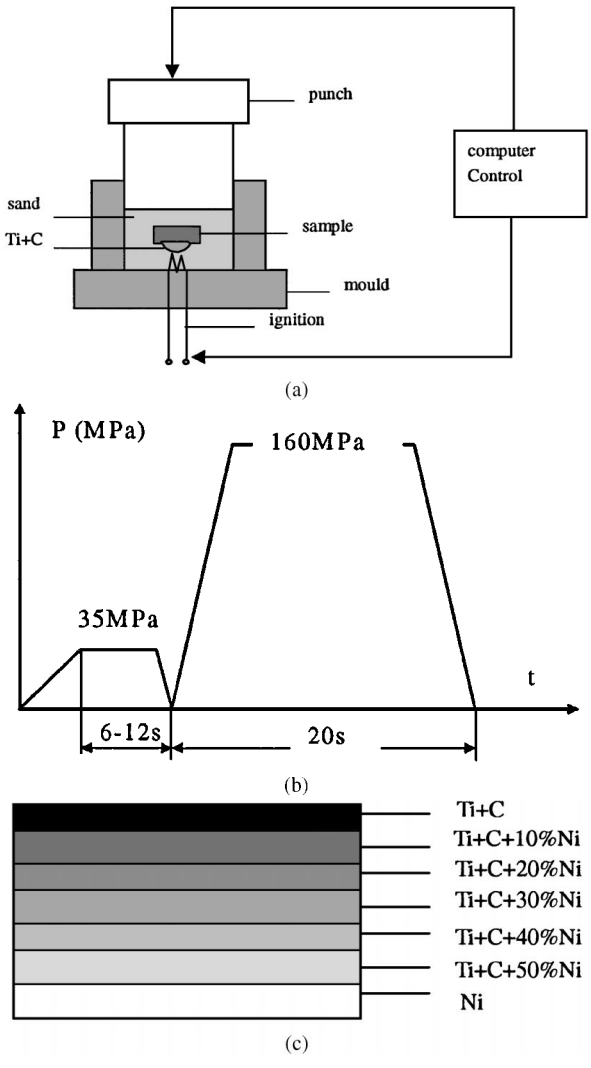

Figure 1 The schematic illustration of simultaneous combustion synthesis and compaction (a) setup; (b) flow chart; (c) powder compacts.

3. Results and discussion

3.1. Composition gradient design

As a result of the differences in material properties, stresses develop in ceramic-metal FGMs which result in plastic deformation of the metal, cracking within the ceramic, or interfacial decohension during fabrication and service. Prior optimization design on FGMs is necessary before fabrication. In this work, finite element analysis was used to model residual stresses developed at graded TiC-Ni interfaces and identity optimum microstructure characteristics for minimizing residual stresses. Considering a $65 \times 65 \times 15$ mm TiC-Ni FGM plate with seven layers as shown in Fig. 2. The values of the property parameters of TiC and Ni employed in the finite element analysis are listed in Table I. It is assumed that no plastic deformation occurs in the specimens and the values of mechanical and thermal properties do not change with the given temperature (773–2073 K). A FGM specimen was divided into 3000 finite elements and 3751 nodes. The following composition gradient was chosen to analyzed the thermal stresses:

$$C_1 = \begin{cases} 0 & 0 \le z \le 1 \\ \left(\dfrac{z-1}{t}\right)^p & 1 < z < 14 \\ 1 & 14 \le z \le 15 \end{cases}$$

TABLE I Data for the mechanical and thermal properties of TiC and Ni

	Young's modulus E (GPa)	Thermal expansion coefficient α ($\times 10^{-6}$/K)	Poisson's ratio γ	Shear modulus G (GPa)
TiC	460	7.4	0.336	172.16
Ni	199.5	18	0.312	76.03

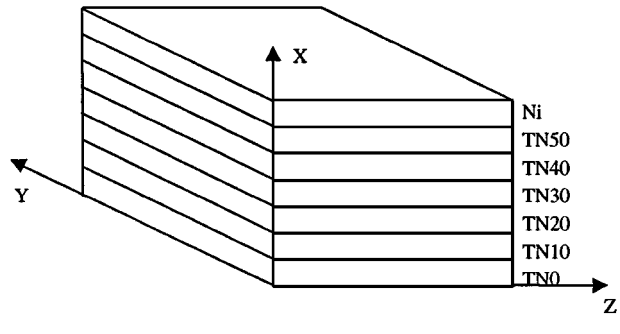

Figure 2 TiC-Ni FGM model.

where C_1 is the weight fraction of Ni, p is the compositional distribution exponent, z is the distance variable, and t is the thickness of the interlayer. The material properties of the TiC-Ni composite as composition of Ni content are determined by the rule of mixtures and empirical modified law of mixtures [9]

$$\alpha = \alpha_1 C_1 + \alpha_2 C_2 \qquad \gamma = \gamma_1 C_1 + \gamma_2 C_2$$
$$E = \frac{(C_2 E_2[(q + E_1)/(q + E_2)] + C_1 E_1)}{(C_2[(q + E_1)/(q + E_2)] + C_1)}$$

where C_1 and C_2 are the weight fraction of Ni and TiC, respectively, $C_1 + C_2 = 1$, q is a constant determined by experiment and is about 4500 MPa for TiC-Ni composites. The FEA results reveal that the residual stresses on the metal/ceramic interface of non-FGM are very high (3508.3 MPa) and will easily result in rupture of the TiC layer. For the TiC-Ni FGM, the values of maximum tension are given in Fig. 3a. It can be seen that the maximum tension initially decreases with a increase in P and then increases with P after passing through a minimum of 684.29 MPa at $P = 0.8$. Compared to a TiC-Ni non-FGM, the maximum values for TiC-Ni FGM with $P = 0.8$ and $P = 1.4$ decrease by 80.5% and 74.1%, respectively. At $P = 0.8$–1.4, the thermal stress relaxation is at an optiminum value, which is less than the strength of TiC (1 GPa). Combined with the maximum tension in TiC and the position of maximum tension with increasing P in Fig. 3b and c, an optiminum value $P = 1.0$ for TiC-Ni FGM can be concluded.

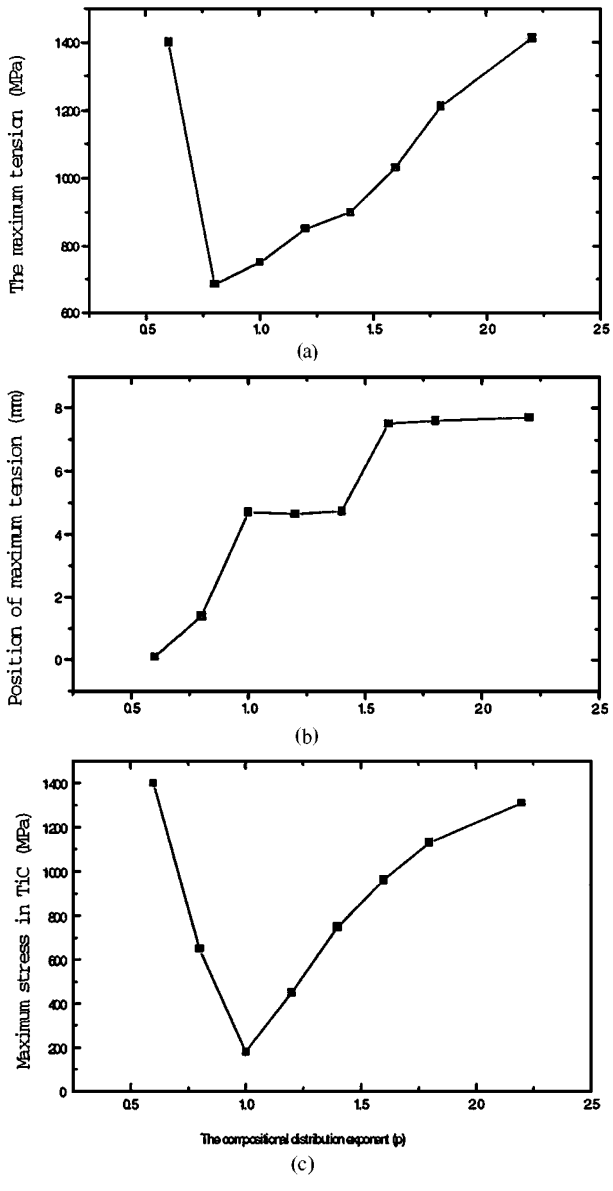

Figure 3 The variation of (a) the maximum tension and (b) its position in the sample, and (c) the maximum tension in TiC with the compositional distribution exponent p.

3.2. Microstructure and metal binder distribution

The X-ray diffraction pattern of TiC-Ni composites indicated that the phase composition consisted of TiC and Ni only as shown in Fig. 4. It is clear that the reaction between Ti and C was complete and no intermediate compounds were detected. With the variation of Ni content, the ratio of TiC and Ni phases changed. The microstructure of the cross section in the functionally graded TiC-Ni material is shown in Fig. 5. The white phase is Ni and dark one is TiC. It is observed that the microstructure is gradually changed from one side to the other side and no distinct boundaries are exhibited. Even on the pre-stacked section where chemical compositions were varied in a stepwise way, both Ni and TiC components are continuous in the microstructure. Fig. 5b shows the microstructure of the cross-section in TiC-xNi composites with different Ni additions. The TiC grain size was decreased with an increasing amount of Ni binder from 10 to 50 wt%. Typical network structures of Ni can be seen in the microstructure for the TiC-Ni with more than 30 wt% Ni. It is noted here that the networks for metal and ceramics are spatially conjugated to each other. During TiC-xNi cermet processing by the combustion synthesis and compaction technique, the molten Ni wets, flows and solidifies at the surface of TiC particles. The microstructure depends upon the Ni content. For the TiC-30Ni material, the microstructure is seen to loose connectivity of the metal phase and shows partially agglomerated TiC grains. These characteristics also can

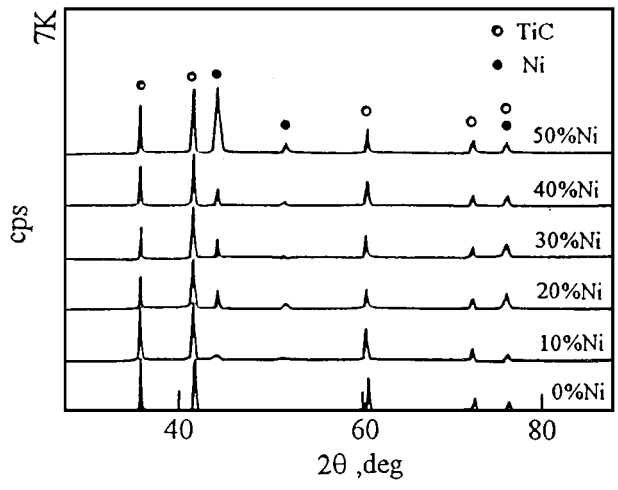

Figure 4 The X-ray diffraction pattern of TiC-Ni composites.

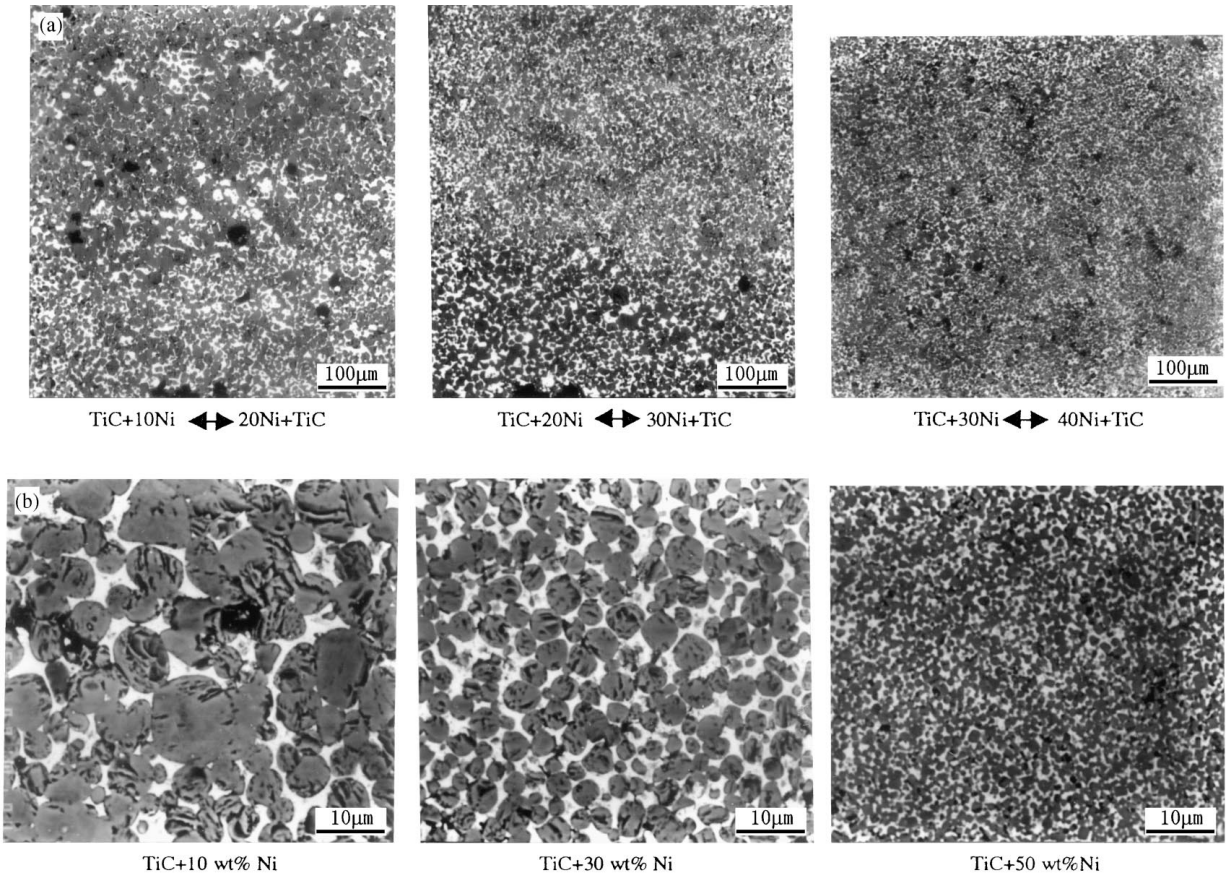

Figure 5 The microstructure of a cross section in (a) TiC-Ni FGM and (b) TiC-Ni composites.

be observed in the microstructure of TiC-Ni FGM in which the microstructure changes from a dispersion composite structure into a network structure as the content of Ni addition increases. An EPMA line analysis of nickel was also performed on the cross-section and a typical distribution of the metal binder is shown in Fig. 6. The intensity changes with the composition gradient well and meets the expected design in the main.

3.3. Mechanical properties

Figs 4 and 5 reveal that the TiC-Ni FGM and non-FGM contained few pores and seemed to be almost fully densified. As show in Fig. 7, the density of TiC-Ni composite increases with the rise of Ni content due to the higher density of Ni (8.85 g/cm^3) compared with TiC (4.93 g/cm^3). The introduction of Ni into TiC-Ni cermets results in a drastic increase in the relative densities. First, the relative densities reached a maximum value at 20 wt% Ni addition and then decreased with increasing Ni. It is clear that the change of densities is not linear with composition. Fig. 8 illustrates the typical hardness depth profile of a TiC-Ni FGM and three point bending strength of TiC-Ni composite with different Ni content. At the lower Ni contents, the molten Ni wets and flows at the surface of TiC grains, and promotes the densification of TiC-Ni composites. The hardness and flexure strength increase with increasing Ni content with the maximum value obtained at about

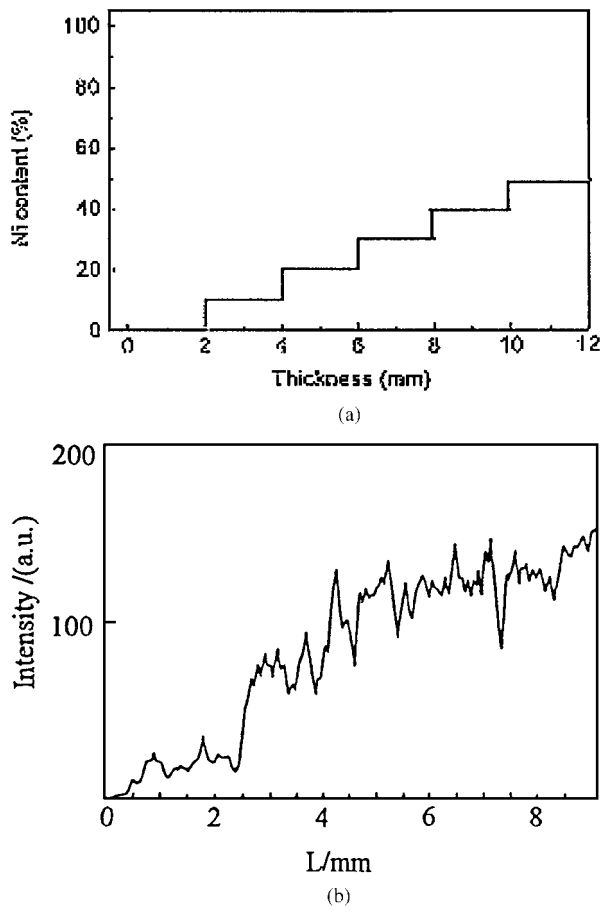

Figure 6 The Ni distribution along the thickness (a) pre-stacked; (b) EPMA profile.

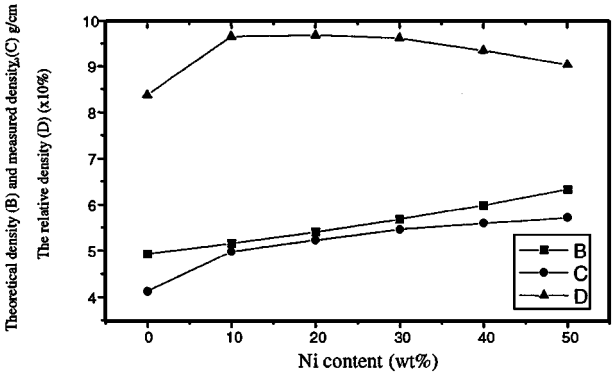

Figure 7 The variation of the densities of TiC-Ni composites as a function of Ni.

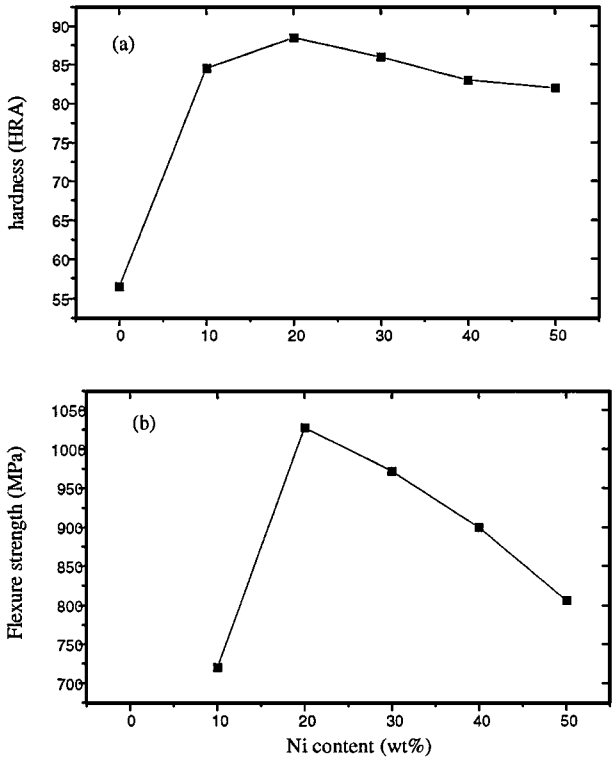

Figure 8 (a) A typical hardness depth profile of TiC-Ni FGM and (b) flexure strength of TiC-Ni composites for different Ni contents.

20 wt% Ni. After that, the decrease of the relative density and the transition of Ni metal phase from a dispersive to connective distribution occur, the Ni phase behaves here as porosity and defects for its low strength. As a result, the hardness and flexure strength decrease with the increase in Ni content. The fracture toughness and Young's modulus was measured and the results are shown in Fig. 9. It is clear that the Young's modulus decreases with increasing the concentration of the Ni metal phase. Combined with the results shown in Figs 7 and 8, the fracture toughness can be seen to increase up to the maximum value 7.41 $MPa \cdot m^{1/2}$ at 30 wt% Ni as the metal binder content increases. This is due to the toughing of Ni phase in TiC-Ni composites. Above 30 wt% Ni, the fracture tougness decreases with the Ni content, matching the change of the relative densities, hardness and flexure strength in Figs 7 and 8.

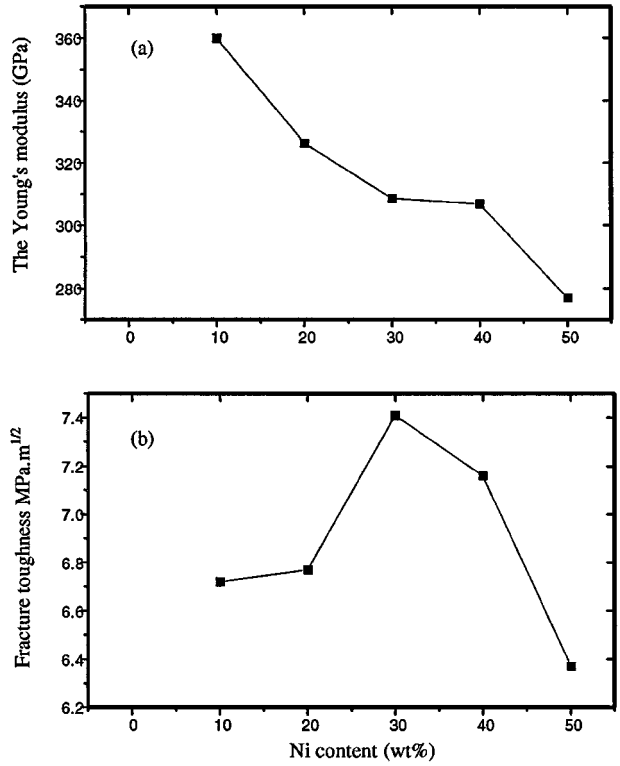

Figure 9 The variation of (a) Young's modulus and (b) fracture toughness with Ni content.

4. Conclusions

1. Fully dense TiC-Ni FGMs and composites have been fabricated using a combination of combustion synthesis and hot compaction of Ti, C and Ni powders. The FGM with the optimized composition gradient consisted of seven layers with varying nickel contents in the different layers varied from 0 to 100%.

2. The TiC-Ni composite consists of Ni and TiC only with no intermediate Ni-Ti compounds. The TiC-Ni FGM has a continous gradient distribution in composition and structure with no distinct interfaces in the FGM even where chemical compositions were made in a stepwise way.

3. The mechanical properties strongly depend on the relative densities and the Ni contents. The hardness, flexure strength and fracture toughness increases initially and then decreases with increasing Ni content. The hardness and flexure strength reach a maximum value at approximately 20 wt% Ni, and fracture toughness at 30 wt% Ni. The Young's modulus decreases with increasing Ni content.

Acknowledgements

This work was supported in part by the Royal Society, and in part by the Excellent Young Investigator Foundation, Department of Education, China.

References

1. S. SAMPATH, H. HERMAN, N. SHIMODA and T. SAITO, *MRS Bull.* **20** (1995) 27.
2. J. ZHU, Z. YIN and Z. LAI, *J. Mater. Sci. Technol.* **10** (1994) 188.
3. Y. MIYAMOTO, *Am. Ceram. Soc. Bull.* **69** (1990) 686.

4. N. SATA, N. SANADA, T. HIRANO and M. NIINO, in "Combustion and Plasma Synthesis of High Temperature Materials," edited by Z. A. Munir and J. B. Holt (VCH, Weinheim, 1990) p. 195.
5. X. MA, K. TANIHATA and Y. MIYAMOTO, *Ceram. Engng. Sci. Proc.* **13** (1992) 356.
6. R. KUDESIA, S. E. NIEDZIALEK and G. C. STANGLE, *ibid.* **13** (1992) 374.
7. I. J. SHON and Z. A. MUNIR, *J. Amer Ceram. Soc.* **81** (1998) 3243.
8. D. PADMAVARDHANI, A. GOMEZ and R. ABBASCHIAN, *Intermetallics* **6** (1998) 229.
9. A. J. MARKWORTH, K. S. RAMESH and W. P. JR. PARKS, *J. Mater. Sci.* **30** (1995) 2183.

Received 12 February
and accepted 11 August 1999